Original Article

Study of the wear of MgO-C refractory in the slag line of steel ladles

Edgard Marcos Ribeiro [1*]
Marcos Vinicius Ribeiro da Cunha [1]
Natália de Castro Bicalho [1]
Rafael Ferreira Delfim Bueno [1]
Helton Jackson Costa [1]
Alamar Kasan Duarte [2]
Vinicius dos Santos Ribeiro [2]
Débora Guimarães da Silva [3]
Wander Luiz Vasconcelos [4]

Abstract

The refractory wear in the slag line of steel ladles is a key factor in steelmaking operations. Understanding the characteristics of the refractory materials used in this region and their interactions with the process is essential for safe operation and optimized performance. In this context, the objective of this study was to evaluate the microstructure of different refractory materials applied to the slag line of steel ladles, identifying the types of magnesia used in each material, the presence of antioxidants, physical properties, and the interaction of each with two typical types of secondary refining slags. Six different commercial brands of MgO-C refractory materials were analyzed through laboratory tests, including chemical analysis, bulk density and apparent porosity and cold crushing strength (CCS), both in the as-received condition and after exposure to 1400 °C for 1 hour in a reducing atmosphere, oxidation resistance, and static corrosion tests. Refractory materials composed exclusively of fused magnesia grains, with larger crystal sizes and a well-distributed graphite matrix, demonstrated greater resistance to chemical attack by slags.

Keywords: Steel ladle; Slag line; Magnesia-carbon refractory (MgO-C); Corrosive wear.

1 Introduction

During the steel production process in a steelmaking plant, the molten metal from the primary refining stage is poured into steel ladles, which are the equipment used in the secondary refining stage. Secondary metallurgy is responsible for the fine adjustment of chemical composition, temperature, and cleanliness, carried out after primary refining [1]. In this process, it is possible to adjust and homogenize the steel both chemically and thermally, remove or modify inclusions, adjust chemical composition, and perform desulfurization or dephosphorization. The slag from primary refining contains high levels of metallic oxides that can lead to non-metallic inclusions, which is undesirable for the subsequent process. However, the presence of slag in the ladle is essential for protecting the steel from oxidation, capturing inclusions, and heating the molten bath through heat transfer via slag/molten metal contact.

The refractory materials applied to the slag line of steel ladles are the focus of this study, and understanding their properties and interactions with the process is essential for safe operation and optimized performance. Steel ladles are equipment internally lined with refractory materials and perform the functions of handling molten metal, removing impurities from the steel, adding alloying elements, and homogenizing temperature and chemical composition. The type of refractory material to be applied to the ladle depends on several factors and is defined by each company according to the requirements of its internal processes [2]. A typical schematic showing the main regions can be seen in Figure 1a. Figure 1b shows the main stresses experienced by the refractories according to the ladle region. It can be observed that in the slag line region, the related wear factors are corrosion, oxidation, and erosion.

[1] *ArcelorMittal, João Monlevade, MG, Brasil.*
[2] *REFRALAB, Santa Luzia, MG, Brasil.*
[3] *Universidade Federal de Minas Gerais - UFMG, Belo Horizonte, MG, Brasil.*
[4] *Departamento de Engenharia Metalúrgica e de Materiais, Universidade Federal de Minas Gerais - UFMG, Belo Horizonte, MG, Brasil.*

[*] *Corresponding author:* edgard.ribeiro@arcelormittal.com.br
E-mails: marcos.cunha@arcelormittal.com.br; natalia.bicalho@arcelormittal.com.br; rafael.f.bueno@arcelormittal.com; helton.costa@arcelormittal.com.br; alamarkasan@gmail.com; vinicius.refralab@gmail.com; debora-g-s@hotmail.com; wlv@demet.ufmg.br

1.1 Properties of refractory materials

The refractory materials applied to a ladle are subjected to various stresses, with the slag line region being the most critical. The main properties required for the materials applied in this area include low apparent porosity, high refractoriness, high oxidation resistance, high corrosion resistance, and good thermal shock resistance [6,7].

1.2 Raw materials

The selection of the refractory material with the best properties for application in the slag line is a key factor. Understanding the different properties resulting from the raw materials chosen for the manufacture of the refractory can be a differentiating factor in performance outcomes.

1.2.1 Magnesia – MgO

Magnesia or magnesium oxide (MgO) is the main raw material used in the production of basic refractories and is available on the market in the form of sintered or fused grains [4,8,9] (Figure 2). Fused grains have higher density, are virtually free of inter and intracrystalline porosity, and contain larger crystals. This results in reduced chemical reactions between the material and the slag, thereby improving the performance of the refractory lining.

MgO sinter aggregates exhibit smaller crystal sizes (Figure 3) compared to fused grains, which can lead to an increased corrosion rate. The higher wear rate of sintered magnesia relative to electrofused magnesia is not only associated with the presence of impurities (CaO and SiO_2) within the magnesia grains, but also with the CaO/SiO_2 ratio (C/S). This ratio plays a critical role in the formation of secondary phases: a low C/S ratio promotes the development of low-melting-point liquid phases, facilitating slag penetration and periclase (MgO) corrosion, whereas an excessively high C/S ratio can result in free CaO, increasing the risk of hydration and compromising structural integrity.

In contrast, electrofused magnesia, despite its lower impurity content, has a reduced internal surface area, which makes it more vulnerable to thermal shock cracking. This occurs because the energy absorbed by the material dissipates through grain boundaries, and the limited presence of such boundaries leads to localized stress and crystal fracture.

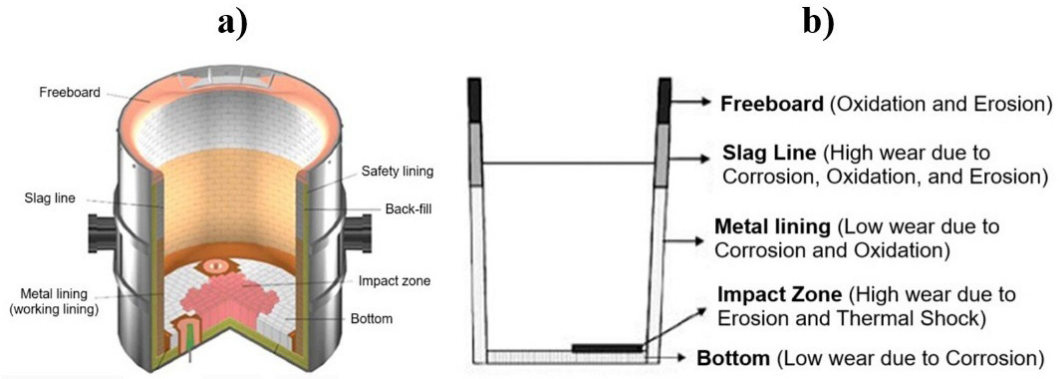

Figure 1. a) Steel ladle and its main regions [adapted from [3]], and b) Zoning of the ladle lining according to wear factors [adapted from [4,5].

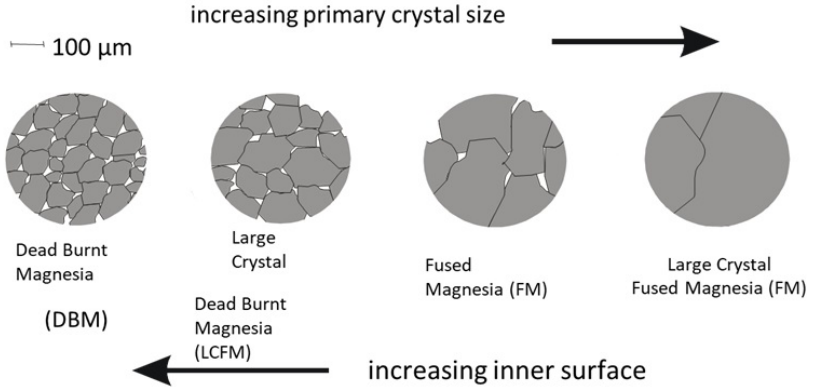

Figure 2. Classification of magnesia according to grain size [9].

Therefore, selecting the appropriate material depends on the dominant wear mechanisms present in each production process.

1.2.2 Carbon

Carbon is an important component of MgO-C refractories (Figure 4) [10]. The main reasons for using carbon in steelmaking refractories are: high refractoriness and thermal stability under non-oxidizing conditions; low wettability by polar liquids, particularly silicate slags; high thermal conductivity; improved resistance to thermal shock; and, when used as a binder, it can easily infiltrate in the porous structure of the refractory material [11].

1.2.3 Antioxidant

The presence of antioxidants is also a relevant factor in the development of certain refractory materials used in steel ladles [5,12,13]. In the upper region of the steel ladle (freeboard), the bricks are exposed to oxidation, and carbon tends to be the most affected in this environment. Therefore, if carbon loss is not properly controlled, the bricks become more friable and susceptible to wear. In the impact zone, bricks containing antioxidants may also be used to increase erosion resistance due to the formation of carbides. The carbides increase the hot modulus of rupture of the bricks.

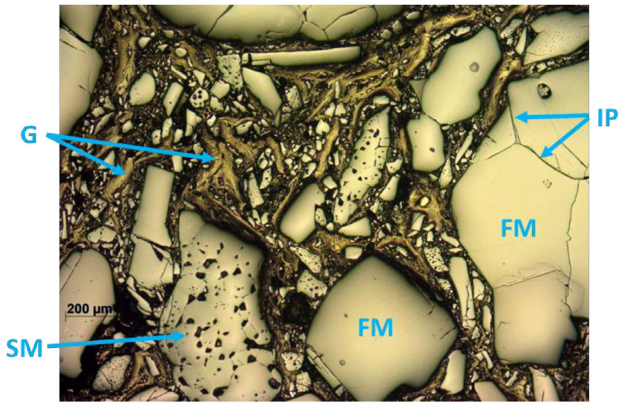

Figure 3. Microstructure of a MgO-C brick, where FM = fused magnesia, SM = sintered magnesia, IP = impurities in the grain boundaries and G = graphite.

1.3 Process influence

The process to which the refractory is subjected imposes conditions of greater stress on the material, potentially leading to high wear rates. One key factor is the operating temperature, since the higher the temperature, the higher the dissolution rate of the refractory. Extended treatment times contribute to corrosion and erosion processes, as they keep the refractory exposed for longer periods. Slags also present a critical factor in refractory wear, related to their basicity and viscosity [14,15]. The CaO/ SiO_2 ratio of the slag has a considerable influence on the wear of the refractory lining in ladles, as demonstrated by its impact on MgO solubility (Figure 5a) [16]. Chemical wear increases non-linearly with decreasing basicity.

MgO–C refractories, are sensitive to slags with high SiO_2 content. SiO_2 reacts with MgO to form forsterite (Mg_2SiO_4), which has a lower melting point than periclase. This phase can dissolve easily into the liquid slag, accelerating corrosion. The higher the SiO_2 content, the greater the fraction of liquid phase, facilitating infiltration, dissolution, and removal of MgO grains.

Slag viscosity directly affects the ability of the liquid phase to dissolve and infiltrate the refractory structure, and consequently, it can either increase or reduce the corrosion rate of these materials. This property varies mainly according to temperature and the concentration of network formers and modifiers (or fluxes) present in the liquid phase.

In both primary and secondary steel refining processes, fluorite (CaF_2) is commonly used to lower the melting point of the slag and improve kinetic conditions for inclusion absorption. However, the presence of CaF_2 acts as a fluxing agent, reducing the consistency of the slag and enhancing its fluidity. More fluid slags penetrate more easily into pores and microcracks within the MgO-C refractory, increasing the corrosion rate, as shown in Figure 5b [17,18].

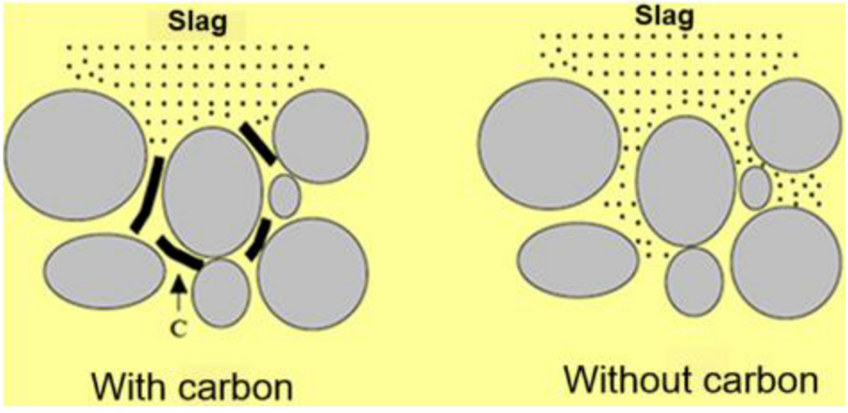

Figure 4. Slag penetration - Effect of graphite on the structure of the refractory material [adapted from [10]].

2 Materials and methods

Samples of slag line refractory bricks from steel ladles supplied by different manufacturers, as well as typical secondary refining slags, were selected for this study. The chemical compositions of the refractory materials are presented in Table 1.

Table 2 shows the results of the chemical analysis of the slags used in the tests. As can be observed, slag A has a low CaO/SiO_2 ratio of 0.62, while slag B has a ratio of 1.34, but with a high fluorite content (27.74%).

2.1 Microstructural characterization

For microstructural characterization, X-ray diffraction, optical microscopy, and scanning electron microscopy techniques were employed on unused refractory samples.

2.2 Bulk density and apparent porosity

The samples were subjected to bulk density and apparent porosity tests both at room temperature and after thermal treatment at 1400 °C for 1 hour, under a reducing atmosphere.

2.3 Cold crushing strength

Cold crushing strength (CCS) was evaluated in two conditions: in the as-received state and after thermal treatment at 1400 °C for 1 hour under a reducing atmosphere. For the heat-treated condition, cylindrical test specimens with dimensions of 50 mm × 50 mm were embedded in a graphite bed, thermally treated, cooled to room temperature, and subsequently tested. The same specimen geometry was used for the as-received condition, ensuring consistent comparison of mechanical performance between the two states.

2.4 Oxidation resistance

Oxidation resistance was measured by exposing the samples to a temperature of 1000 °C for 5 hours, with air flowing through the furnace. After cooling, the specimens were cut in the middle for the evaluation of the oxidized (decarbonized) layer, and the oxidation percentage of each material was determined. The tests were conducted on cylindrical specimens with dimensions of 50 mm diameter x 50 mm height.

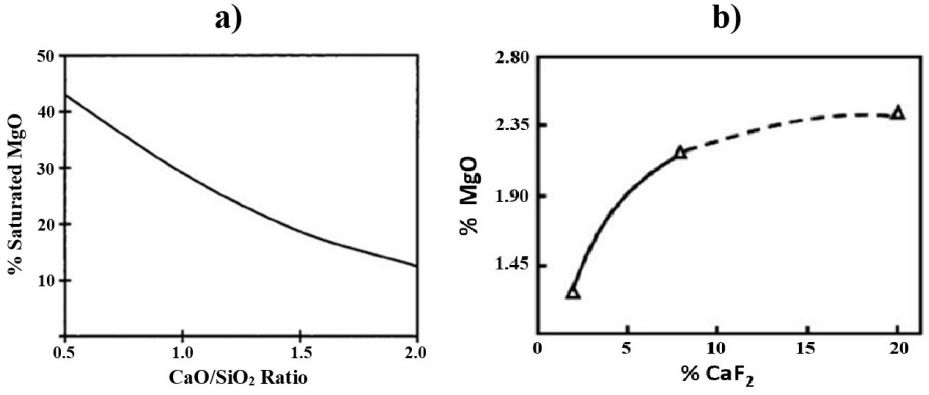

Figure 5. a) Effect of CaO/SiO_2 ratio (basicity) on the solubility of MgO in the slag [adapted from [16]]; and b) Effect of fluorite (CaF_2) addition on the solubility of MgO in the slag [adapted from [18].

Table 1. Chemical composition of different samples of refractory materials applied to the slag line of steel ladles

Sample	C	CaO	SiO_2	Al_2O_3	Fe_2O_3	Cr_2O_3	MgO	MnO
T1	10.07	1.26	0.60	0.23	0.66	0.01	97.16	0.07
T2	9.74	1.19	0.56	0.19	0.46	0.01	97.51	0.07
T3	13.46	1.20	5.57	0.30	0.82	0.04	92.01	0.04
T4	12.60	1.01	0.84	0.70	0.88	0.10	96.38	0.08
T5	12.65	1.89	1.56	<0.01	0.22	0.01	96.22	0.10
T6	12.93	1.04	1.22	0.29	1.14	<0.01	96.24	0.05

The Na_2O, K_2O, P_2O_5, and TiO_2 values for all samples were below 0.01%.

Table 2. Chemical composition of two typical secondary refining slags

Slag	CaO	SiO_2	Al_2O_3	MgO	Fe_2O_3	K_2O	Cr_2O_3	P_2O_5	CaF_2	CaO/SiO_2
A	30.01	48.35	2.49	13.98	4.07	0.2	0.19	0.12	<0.41	0.62
B	27.93	20.92	6.10	11.10	3.65	1.19	0.05	0.30	27.74	1.34

MnO, Na_2O, and TiO_2 values for all samples were residual.

The oxidation result is based on the calculation of the initial surface area of the sample minus the non-decarbonized area of the final sample. The difference between these values is divided by the initial area, resulting in the oxidation percentage for each material.

2.5 Slag attack resistance

Test specimens of the refractory materials were prepared according to NBR 9641, with central holes drilled in the samples for the deposition of two different types of typical secondary refining slags. These slag-containing specimens were heated to 1600 °C for 1 hour (under oxidizing atmosphere). After the test, the specimens were naturally cooled down to room temperature and cut in the middle to evaluate the wear they experienced (Figure 6).

3 Results and discussion

3.1 Microstructural characterization

Optical microscopy and scanning electron microscopy (SEM) analyses with EDS chemical mapping were performed for all samples.

For sample T1, the optical microscopy and SEM images presented in Figure 7 reveal the presence of high-quality electrofused grains, characterized by magnesia crystal sizes exceeding 400 µm. The microstructure consists of a matrix exclusively composed of electrofused magnesia, exhibiting well-defined graphite veins. Furthermore, the SEM analysis indicates the occurrence of a secondary phase containing Ca and Si located between two magnesia crystals, although its concentration remains low throughout the structure.

For sample T2 (Figure 8), the presence of high-quality electrofused grains is also observed, with magnesia crystal sizes above 400 µm, and a matrix composed exclusively of electrofused magnesia, featuring well-defined graphite veins. The SEM image also shows a secondary phase containing Ca and Si between magnesia crystals, although with low concentrations throughout the structure.

For sample T3 (Figure 9), optical and electron microscopy revealed the presence of both low- and high-quality electrofused grains. Optical microscopy shows that, despite the large magnesia grain size (greater than 800 µm), the magnesia crystal sizes are smaller or equal to 200 µm, with a high concentration of impurities between the crystals. As observed in the SEM image, the structure also contains electrofused magnesia with larger crystals and lower impurity content. Overall, the sample predominantly exhibits smaller crystals. Furthermore, a considerable presence of metallic Si was detected in the magnesia-graphite matrix, which was used as an antioxidant element.

For sample T4 (Figure 10), the images show the presence of both electrofused and sintered magnesia grains (identified in the main periclase grains as well as in the matrix). A secondary phase containing Ca and Si is observed throughout the structure, including inside the sintered magnesia grain. No metallic element used as an antioxidant was detected.

For sample T5 (Figure 11), the images presented show the presence of high-quality electrofused grains, with magnesia crystal sizes above 400 µm, a matrix containing only electrofused magnesia, and well-defined graphite veins. The SEM image also reveals the presence of metallic Si in the magnesia and graphite matrix, which was used as an antioxidant element. Compared to sample T3, the percentage of metallic Si appears in smaller proportions.

For sample T6 (Figure 12), optical and electron microscopy revealed the presence of electro-fused and sintered

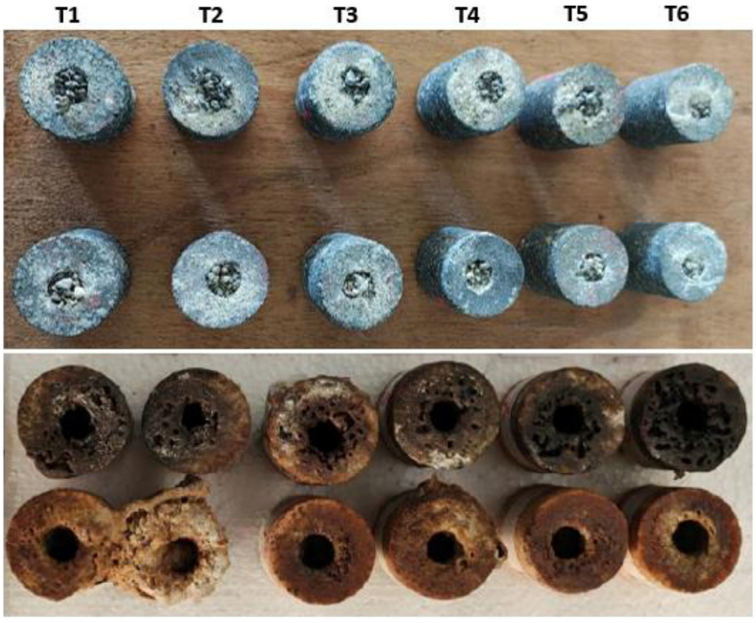

Figure 6. Specimens before (upper) and after the static slagging test (lower).

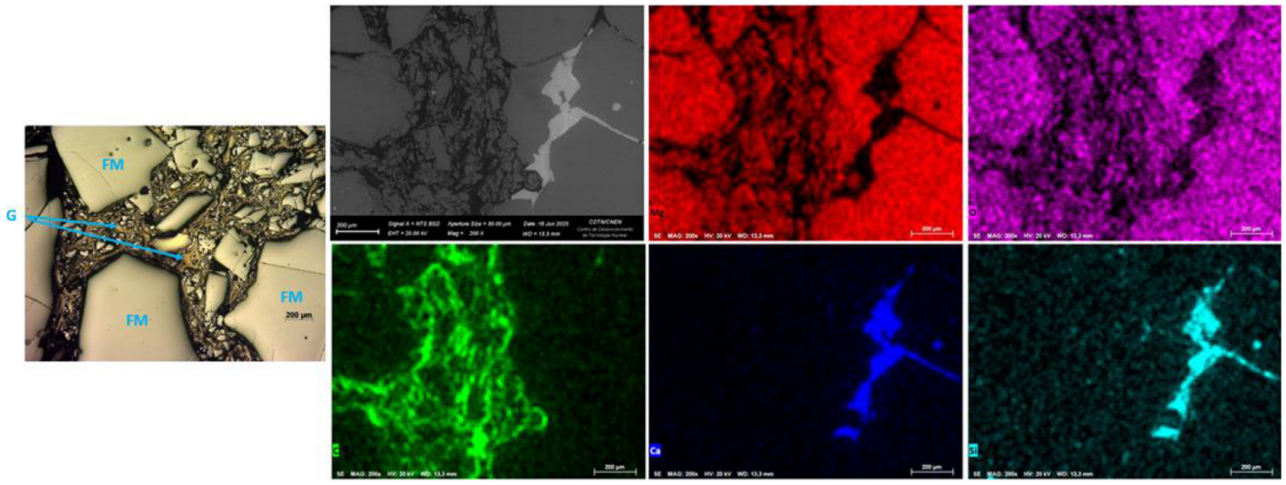

Figure 7. Optical microscopy and scanning electron microscopy with EDS chemical mapping of sample T1, where FM = fused magnesia and G = graphite.

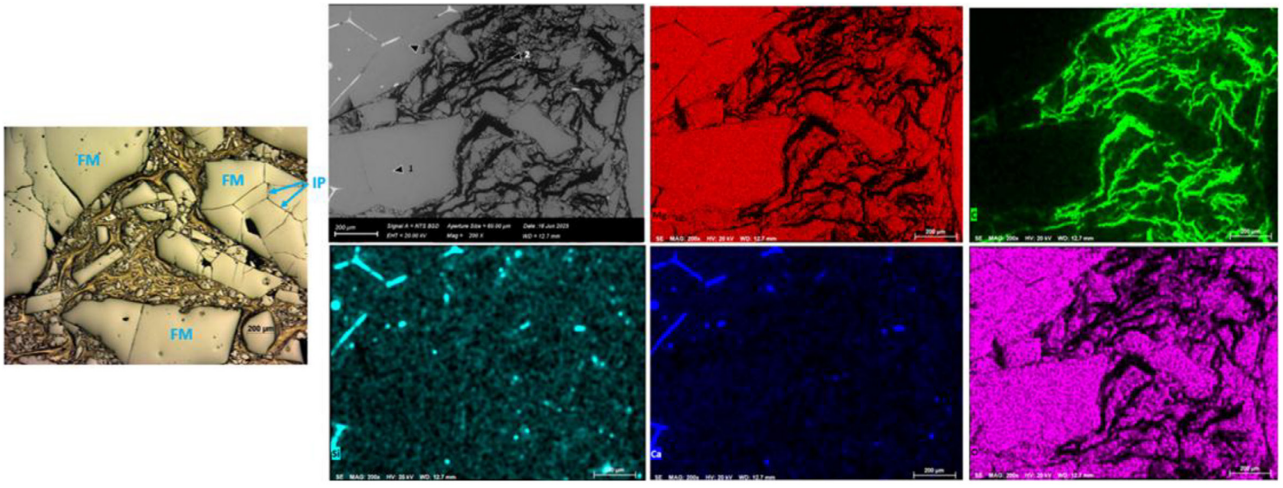

Figure 8. Optical microscopy and scanning electron microscopy with EDS chemical mapping of sample T2, where FM = fused magnesia and IP = impurities in the grain boundaries.

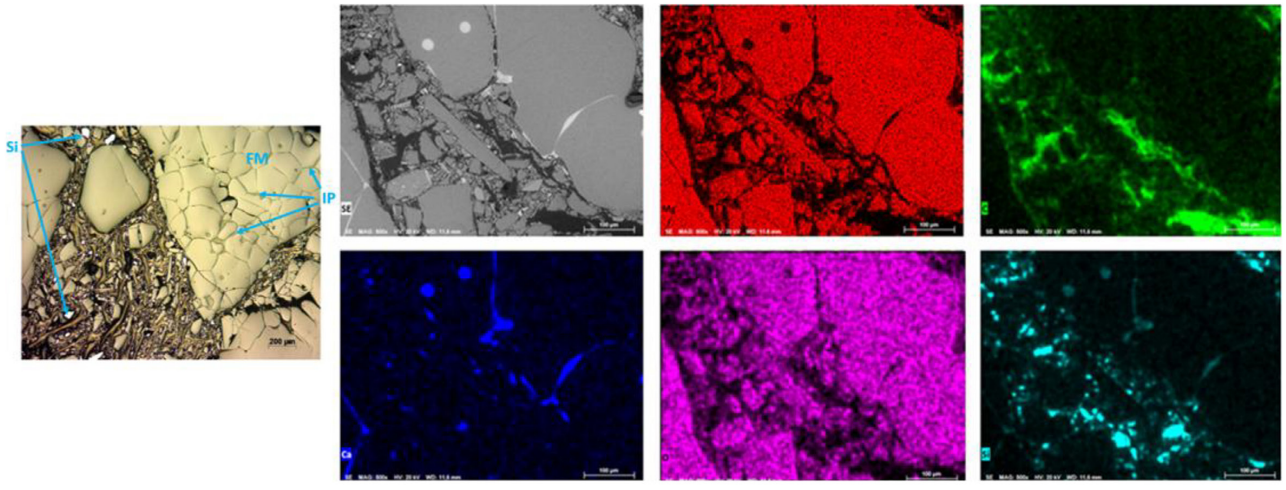

Figure 9. Optical microscopy and scanning electron microscopy with EDS chemical mapping of sample T3, where FM = fused magnesia, IP = impurities in the grain boundaries, and Si = metallic silicon.

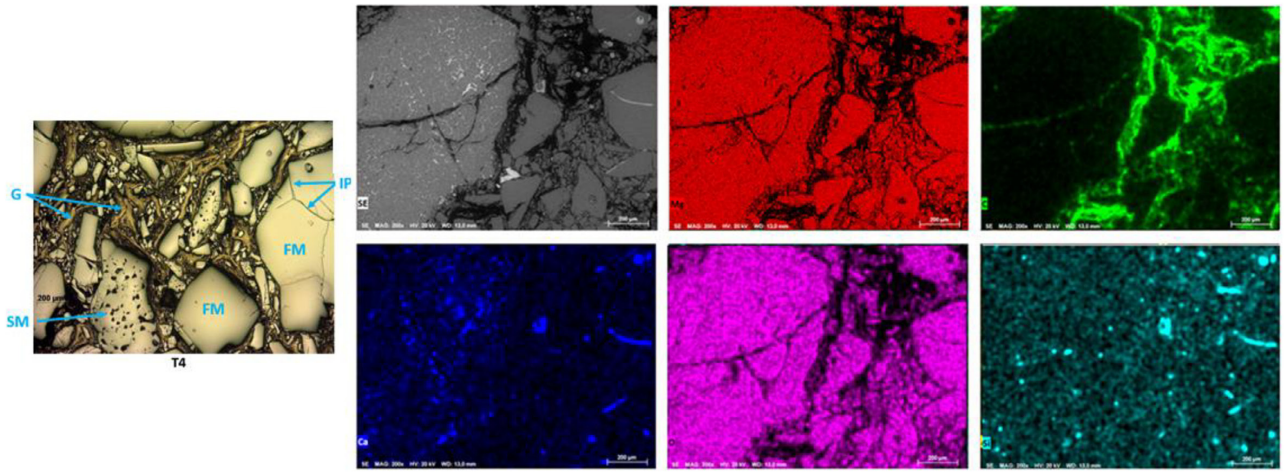

Figure 10. Optical microscopy and scanning electron microscopy with EDS chemical mapping of sample T4, where FM = fused magnesia, SM = sintered magnesia, IP = impurities in the grain boundaries, and G = graphite.

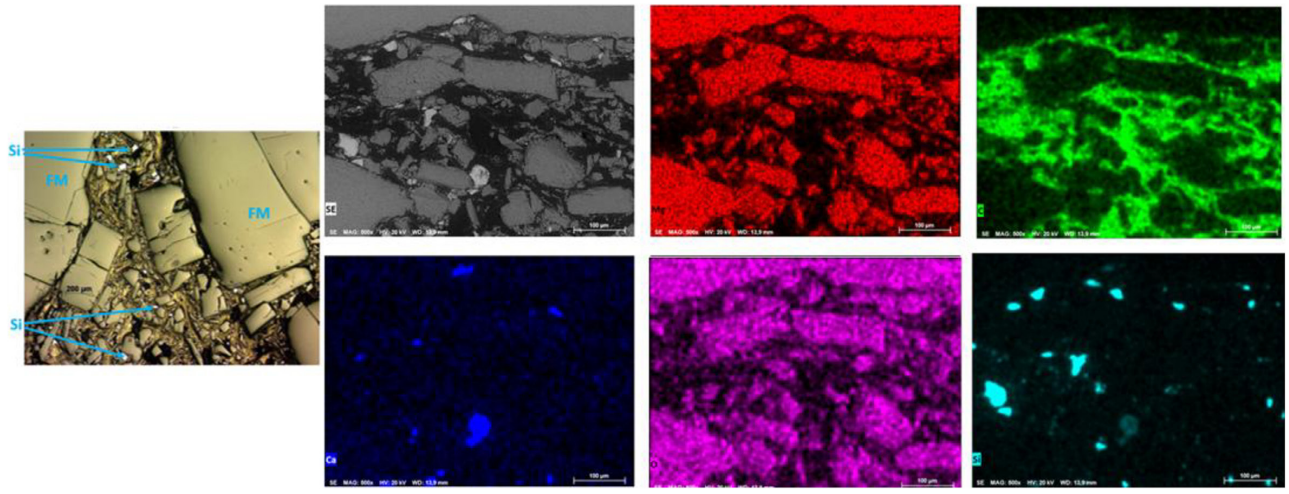

Figure 11. Optical microscopy and scanning electron microscopy with chemical mapping by EDS of sample T5, where FM = fused magnesia and Si = metallic silicon.

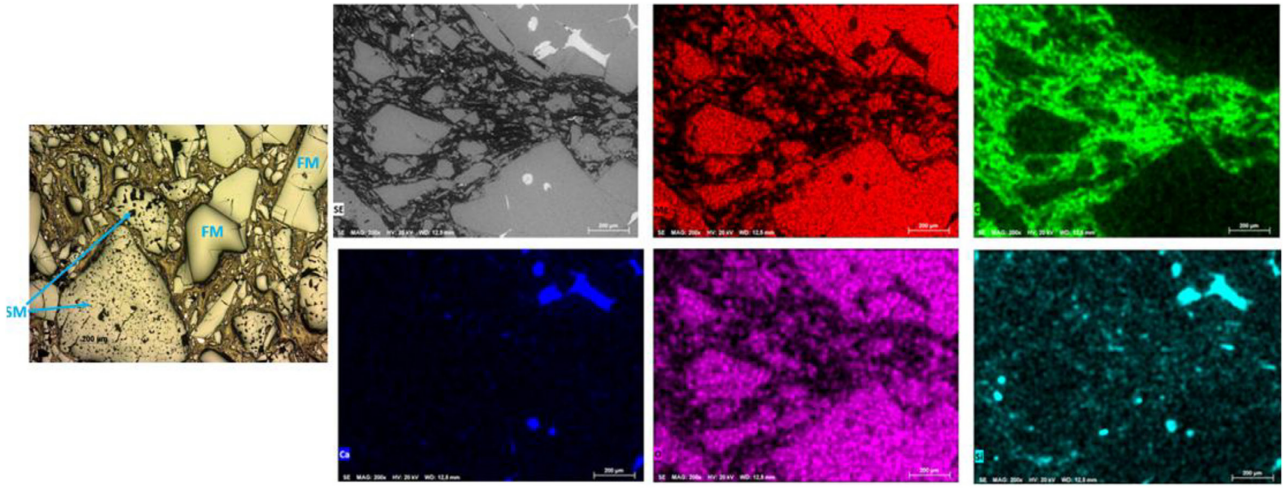

Figure 12. Optical microscopy and scanning electron microscopy with chemical mapping by EDS of sample T6, where FM = fused magnesia and SM = sintered magnesia.

magnesia grains, with the latter being in greater proportion in sample T6 compared to the other materials. The sintered magnesia was identified both in the main periclase grains and in the matrix. A secondary phase containing Ca and Si was observed between the magnesia crystals. No metallic element used as an antioxidant was detected.

Microstructural characterization indicated that not all evaluated materials were exclusively composed of high-quality electro-fused magnesia grains. Sintered MgO was also detected in variable concentrations. The microstructural analyses presented in this study demonstrated that samples T4 and T6 contained sintered magnesia grains within their structure. In samples T3 and T5, metallic silicon was identified as an antioxidant additive, occurring in higher proportion in sample T3. Samples T1, T2, and T5 exhibited only electro-fused magnesia grains.

3.2 Bulk density, apparent porosity and cold crushing strength

Table 3 shows the results for bulk density, apparent porosity, and cold crushing strength (CCS). It is noted that the bulk density results present a low dispersion in the unused material and after heat treatment at 1400 °C/1h under reducing atmosphere. However, the porosity results show greater variations, both in the unused samples and after treatment.

Considering the post-treatment condition, which better reflects the actual state of the material, a difference of up to 20% was observed in porosity results.

Magnesia–carbon (MgO–C) refractories tend to lose mechanical strength and bulk density after heat treatment because the carbon present in the matrix oxidizes at high temperatures, generating increased porosity, microcracks, and a reduction in cohesion between MgO grains. This process removes part of the carbon that previously contributed to the structural integrity of the material, resulting in a more porous microstructure with lower mechanical robustness.

Another contributing factor is the presence of impurities such as CaO and SiO_2 in magnesia aggregates, which tend to concentrate along grain boundaries and form low-melting-point phases that become liquid during heating. This liquid phase intensifies void formation and consequently increases porosity, leading to a reduction in both bulk density and mechanical strength of the refractory.

Samples T3, T4 and T6, exhibited the greatest increase in porosity when comparing the as-received condition with the heat-treated condition. This behavior is likely associated with the previously discussed factors of carbon oxidation and the higher percentage of impurities, as observed in the microstructures, with the identification of sintered grains (samples T4 and T6) and smaller electrofused magnesia crystals containing a greater presence of impurities along the grain boundaries (sample T3).

3.3 Oxidation resistance

Figure 13 shows the samples after the oxidation test.

Figure 14 shows that materials T5 and T3 presented the lowest oxidation rates, due to the presence of metallic Si as an antioxidant. The other materials showed higher oxidation rates, mainly materials T1 and T2. However, the observed values are acceptable for materials that do not contain antioxidants.

Table 3. Results of bulk density, apparent porosity and cold crushing strength

	Sample	T1	T2	T3	T4	T5	T6
As-received (unused refractories)	Bulk density, g/cm³	3.12±0.01	3.15±0.01	3.03±0.04	3.08±0.05	3.04±0.01	3.13±0.01
	Apparent porosity (%)	2.7±0.4	2.1±0.1	1.8±0.3	1.3±0.7	3.3±0.1	1.1±0.3
	CCS, MPa	31.1±5.3	39.7±7.2	33.9±4.6	35.3±3.2	45.24±2.2	32.5±7.8
After heat treatment 1400 °C	Bulk density, g/cm³	2.97±0.04	3.06±0.01	2.93±0.01	2.89±0.06	2.97±0.00	3.02±0.01
	Apparent porosity (%)	8.7±0.6	7.4±0.6	7.8±0.3	8.6±0.6	7.3±0.0	6.6±1.2
	CCS, MPa	11.2±1.2	16.0±4.4	19.3±6.6	17.9±2.8	19.0±4.7	12.3±2.0

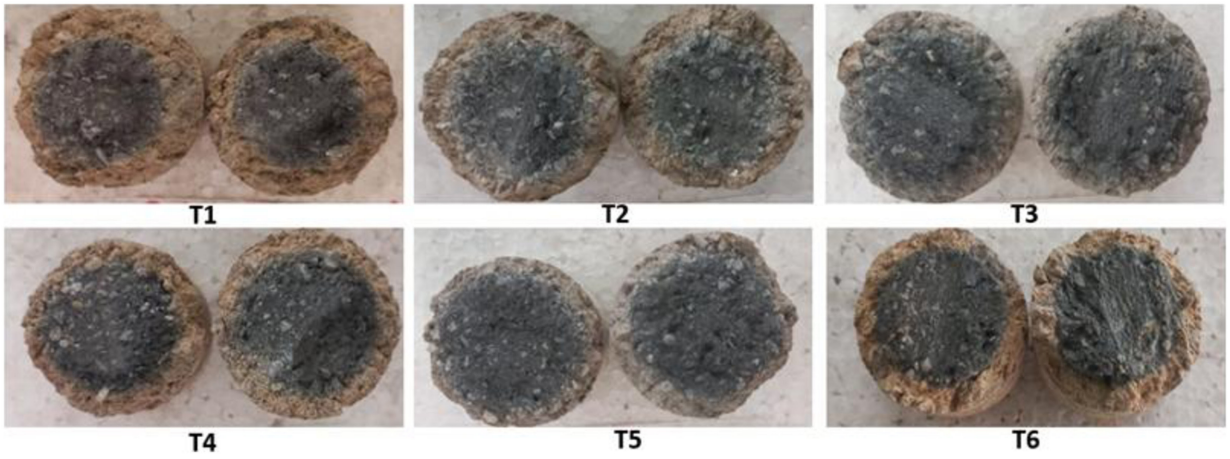

Figure 13. Samples after oxidation resistance test.

3.4 Resistance to slag wear

Figure 15 illustrates the refractory samples cut in the middle for evaluation and measurement of the area worn by slag.

The wear result from the static corrosion test is shown in Figure 16.

Material T5 showed the highest resistance to slag attack (average test result), followed by materials T1 and T2. This result correlates with the microstructure observed in the materials, which consisted only of fused magnesia grains with larger crystal sizes. Materials containing sintered magnesia and predominantly smaller crystal sizes exhibited a higher percentage of wear.

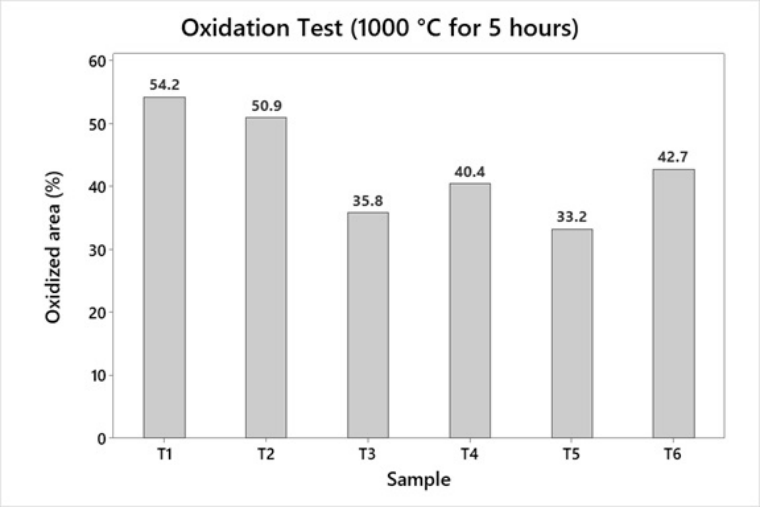

Figure 14. Result of the oxidation resistance test.

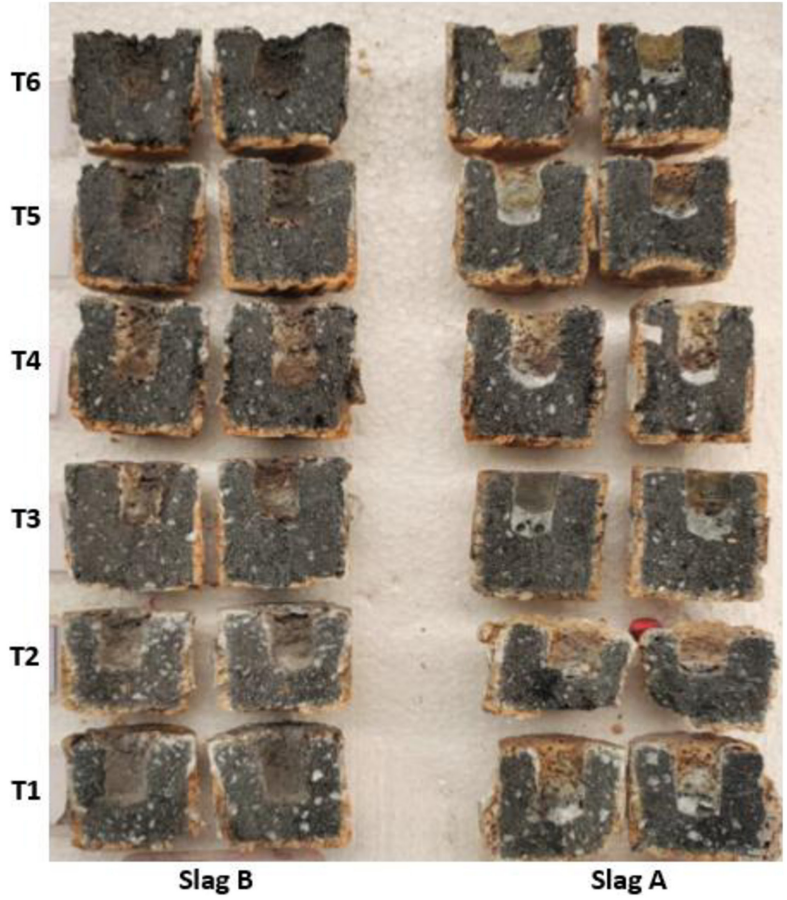

Figure 15. Samples after the static corrosion test.

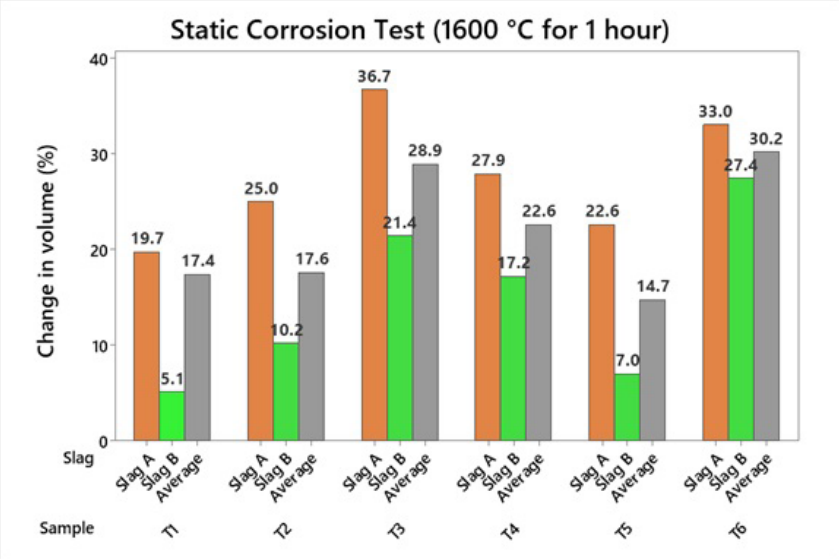

Figure 16. Result of the static corrosion test.

Static corrosion tests indicated that the acidic slag promotes greater wear of the refractories. As previously discussed, the MgO saturation level under low-basicity conditions tends to be higher when compared with the isolated effect of CaF_2 content; for this reason, the chemical wear was more pronounced.

However, it is worth noting that the literature reports that high fluorite contents significantly contribute to refractory degradation due to increased slag wettability, removal of the carbon barrier, and chemical attack on MgO, with consequent formation of MgF_2. This effect could be more accurately evaluated through a dynamic corrosion test or by performing slag-attack trials in an induction furnace.

4 Conclusion

It is observed that there are several materials available on the market with considerable microstructural variation among them. Microstructural characterization studies are essential to validate the information provided in technical data sheets, as well as to understand the practical performance of each of these materials, when used in the steelmaking production process.

The presence of metallic Silicon as an antioxidant proved effective in the oxidation test, as materials T5 and T3 showed the best results.

The slag attack results indicate that materials containing fused magnesia grains, with larger crystal sizes, exhibited lower corrosion rates. This was expected, since larger crystals have a lower surface area, reducing the formation of liquid phase between crystals and hindering slag penetration and, consequently, chemical attack. Materials with a higher percentage of sintered MgO showed poorer performance in the corrosion test.

Static corrosion tests indicated that the acidic slag promotes greater refractory wear, with material T5 showing the highest resistance, followed by T1 and T2. This outcome reinforces the importance of magnesia quality and microstructural characteristics in refractory durability.

Understanding the main wear mechanisms involved in each steel plant's process is a key factor in selecting the most appropriate refractory material for the operation, thus achieving the best performance results.

Acknowledgements

The authors would like to thank ArcelorMittal, Refralab, and UFMG for their support and infrastructure in the development of this work.

References

1 Araújo LA. Manual de siderurgia. 2. ed. São Paulo: Arte e Ciência; 2005.

2 Duarte A. Classificação de Refratários. In: Curso fundamentos de refratários. Belo Horizonte: [s.n.]; 2012.

3 Costa HJ, Ribeiro EM. Curso academia de siderurgia da ArcelorMittal Monlevade. João Monlevade (MG); 2016.

4 Leite FC, Luz AP, Pandolfelli VC. Características e mecanismos de desgaste dos refratários MgO-C usados na linha de escória de panelas de aço. São Carlos (SP): Universidade Federal de São Carlos; 2014.

5 Jansen HW, Daldrup HG. Refractories in steel ladles: materials and design. In: AISTech Conference Proceedings; 2004; Warrendale (PA). Warrendale (PA): Association for Iron & Steel Technology; 2004. Vol. 1.

6 Freire MV, Trujillo JJ, Silva SLC, Costa e Silva ALV. Um enfoque termodinâmico para o estudo do comportamento de refratários MgO-C na linha de escória de panelas para aço líquido. In: Associação Brasileira de Metalurgia, Materiais e Mineração. Anais do 47º Seminário de Aciaria – Internacional, ABM Week; 2016; Rio de Janeiro. São Paulo: ABM; 2016.

7 Kundu R, Sarkar R. MgO-C refractories: a detailed review of these irreplaceable refractories in steelmaking. InterCeram: International Ceramic Review. 2021;70:46-55.

8 Li J, Zhang Y, Shao S, Zhang S. Comparative life cycle assessment of conventional and new fused magnesia production. Journal of Cleaner Production. 2015;91:170-179. https://doi.org/10.1016/j.jclepro.2014.12.043.

9 Duarte AK, Figueiredo AO Jr. Introdução a Refratários. In: Associação Brasileira de Metalurgia, Materiais e Mineração. Refratários para siderurgia. Curso da ABM. São Paulo: ABM; 2023.

10 Duarte AK. Fundamentos em refratários. In: Seminários ALAFAR 2015; 2015; Santiago do Chile. Santiago do Chile; 2015.

11 Zhu T, Li Y, Sang S, Xie Z. A new approach to fabricate MgO-C refractories with high thermal shock resistance by adding artificial graphite. Journal of the European Ceramic Society. 2018;38(4):2179-2185. https://doi.org/10.1016/j.jeurceramsoc.2017.10.018.

12 Luz AP, Souza TM, Pagliosa C, Brito MAM, Pandolfelli VC. In situ hot elastic modulus evolution of MgO–C refractories containing Al, Si or Al–Mg antioxidants. Ceramics International. 2016;42(8):9836-9843. https://doi.org/10.1016/j.ceramint.2016.03.080.

13 Sarkar R. Refractory technology: fundamentals and applications. Boca Raton: CRC Press; 2016. https://doi.org/10.1201/9781315368054.

14 Akkurt S, Leigh HD. Corrosion of MgO-C ladle refractories. Bulletin of the American Ceramic Society. 2003;82(5):9201-9206.

15 Borges RAA, Lenz e Silva GFB. A statistical and post-mortem study of wear and performance of MgO-C resin bonded refractories used on the slag line ladle of a basic oxygen steelmaking plant. Engineering Failure Analysis. 2017;78:161-168. https://doi.org/10.1016/j.engfailanal.2017.03.020.

16 Zhang S, Lee WE. Use of phase diagrams in studies of refractories corrosion. International Materials Reviews. 2000;45(2):41-58. https://doi.org/10.1179/095066000101528304.

17 Bragança SR. Corrosão de refratários utilizados na siderurgia. Parte II: propriedades físicas dos refratários e fatores operacionais. Cerâmica. 2012;58(348):459-464. https://doi.org/10.1590/S0366-69132012000400007.

18 Zhang P, Seetharaman S. Dissolution of MgO in CaO–FeO–CaF_2–SiO_2 slags under static conditions. Journal of the American Ceramic Society. 1994;77(4):970-976. https://doi.org/10.1111/j.1151-2916.1994.tb07254.x.

Received: 28 Oct. 2025
Accepted: 2 Feb. 2026

Editor-in-charge:
André Luiz Vasconcellos da Costa e Silva